



## A new 1,2,3-triazole and its rhodamine B derivatives as a fluorescence probe for mercury ions

Wenying He<sup>a,\*</sup>, Rongqiang Liu<sup>a</sup>, Yuanhao Liao<sup>b</sup>, Guohua Ding<sup>b</sup>, Jianling Li<sup>b</sup>, Wei Liu<sup>a</sup>, Luyong Wu<sup>b</sup>, Huajie Feng<sup>c</sup>, Zaifeng Shi<sup>a</sup>, Mengxiong He<sup>c</sup>

<sup>a</sup> Key Laboratory of Water Pollution Treatment & Resource Reuse of Hainan Province, Haikou, 571158, China

<sup>b</sup> Key Laboratory of Tropical Medicinal Plant Chemistry of Ministry of Education, Haikou, 571158, China

<sup>c</sup> College of Chemistry and Chemical Engineering, Hainan Normal University, Haikou, 571158, China

### ARTICLE INFO

#### Keywords:

5-methyl-1-phenyl-1H-1,2,3-triazole-4-carboxylic acid  
Structural properties  
Rhodamine B  
Colorimetric  
Hg<sup>2+</sup> ion  
Cell imaging

### ABSTRACT

A newly synthesized compound, 5-methyl-1-phenyl-1H-1,2,3-triazole-4-carboxylic acid (MPC) was analyzed for its quantum chemical parameters and theoretical spectrum by computational chemistry. The calculated spectrum was in accord with the experimental measurements in a great degree. Then MPC was successfully designed and synthesized to a novel rhodamine B derivative RMPC. The RMPC exhibited about a 4000-fold increase in fluorescence intensity in the presence of Hg<sup>2+</sup> ions over most other competitive metal ions. The triazole appended colorless chemodosimeter RMPC turns to pink upon the complex formation only with Hg<sup>2+</sup> ions as a 1:2 M ratio and enables naked-eye detection. The coordination mechanism of turning on/off fluorescence for Hg<sup>2+</sup> ions were well proposed by explaining Hg<sup>2+</sup> inducing the ring-opened rhodamine B moiety. The fluorescence imaging experiments of Hg<sup>2+</sup> in HeLa cell demonstrated that the probe was labeled and it could be used in biological systems.

### 1. Introduction

Nitrogen-rich azole heterocycles are promising compounds that fulfill many requirements in many fields with the development of click chemistry, including energetic materials, chemical, biological, macromolecular materials, and pharmaceutical sciences. Owing to less toxic effects, good biological activity, high positive heats of formation resulting from the large number of N–N and C–N bonds and the high level of environmental compatibility, triazole, and tetrazole compounds have been studied over the last couple of years with growing interest [1–3]. Several researches have been reported that 1,2,3-triazoles can also serve as ligands capable of binding to various metal ions and have shown distinct pharmacological activity because of their satisfactory coordination abilities [4–7]. However the overdose or lack of metal ions will harm the human body and organisms. Especially, the contamination of heavy metal ions such as Hg<sup>2+</sup>, As<sup>2+</sup>, Pb<sup>2+</sup>, and Cd<sup>2+</sup> has been becoming one of the most serious problems in the environment because of the increasing industrial and agricultural activities as well as the improper release of metal ions from waste water and domestic effluents [8]. For example, mercury ion (Hg<sup>2+</sup>) is one of the most harmful substances to human beings because of its combination with sulfhydryl groups of proteins in various organs including kidneys, brain, immune

system and central nervous system [9]. How to recognize mercury ions sensitively and efficiently has drawn the more and more interest of researchers. Many studies have been reported on exploiting a wide variety of analytical methods for detecting Hg<sup>2+</sup> [8–12].

Recently, some techniques such as electrochemistry [12], fluorescence spectroscopy [13], atomic absorption spectroscopy (AAS) [14] and inductively coupled plasma mass spectrometry (ICP-MS) [15] have been developed for detection of metal ions. Accordingly, considerable efforts have been devoted to developing fluorescent probes for Hg<sup>2+</sup> because fluorescent detection is the most efficient method, operational simplicity, low cost, real-time monitoring, and high sensitivity [16]. Especially the chromogenic reaction is usually applied to detect and probe analytical species due to it is extremely simple and practical feature. So the colorimetric sensors using the fluorescence analysis method have drawn more and more attention because of many advantages such as fast response, signal visibility, easy operation, and high throughput analysis [17,18]. Among various fluorescent, colorimetric probes, some fluorophores employed as signal reporters of these probes mainly focused on rhodamine, which exhibited the excellent photophysical properties such as high fluorescence quantum yield, large extinction coefficient, long absorption, emission wavelength and high stability against light [19–21]. Generally, rhodamine with a

\* Corresponding author. Key laboratory of Water Pollution Treatment & Resource Reuse of Hainan province, Hainan Normal University, Haikou, 571158, China.  
E-mail address: [hewenying@hainnu.edu.cn](mailto:hewenying@hainnu.edu.cn) (W. He).

particular spirolactam structure is colorless and nonfluorescent. Metal ion can stimulate the spirolactam form to turn into the open-ring forms with pink color and strong fluorescence [22]. The rhodamine B derivatives can exhibit apparent fluorescence enhancement and color changes from the closed-loop state to the open-loop state when binding to various metal ions, which have been broadly utilized to design as “off-on” fluorescent probes for detecting these metal ions [23]. Recent studies on rhodamine-triazoles systems have shown that these complexes could specifically recognize many metal ions such as  $\text{Cu}^{2+}$ ,  $\text{Fe}^{3+}$ ,  $\text{Sn}^{2+}$ ,  $\text{Hg}^{2+}$ ,  $\text{Zn}^{2+}$ ,  $\text{Al}^{3+}$  etc [24–31], which all indicated as a monofunctional probe with different selective and sensitive colorimetric assays.

The different fluorescence probes for mercury ion detection have been reported in a large number of the existing literatures. In consideration of these chemosensors for  $\text{Hg}^{2+}$  ions based on triazole derivatives, there are generally two different modes. On the one hand, these compounds bearing triazole units for recognition of  $\text{Hg}^{2+}$  ions exhibited the fluorescence enhancement or quenching without any variation in colour [32–38]. On the other hand, some probes showed a highly selective and sensitive response as fluorometric and colorimetric sensors towards  $\text{Hg}^{2+}$  ion accompanied by distinct color changes from colorless to pink [39–41], or from yellow to purple [42,43], or from yellow to brownness [44,45], or from yellow to green [46] etc, all of which provided “naked eye” detection of  $\text{Hg}^{2+}$ . Above all, there are several similar aspects such as enhancing the fluorescence signal in methanol or weakly neutral aqueous solution. Also the stoichiometry of the complex formed between  $\text{Hg}^{2+}$  and triazoles is 1:1 or 2: 1 ratio in most cases. The similar results could also be found in our previous studies, which revealed a series of new 1,2,3-triazole appended rhodamine chemosensors for only selective detection of  $\text{Hg}^{2+}$  ions and again proved in the present study [30,31]. Herein, it is indicated that the probe RMPC showed a high selectivity for  $\text{Hg}^{2+}$  ions but a narrower linear range and a lower sensitivity. However, RMPC is an advancement for the application of 1,2,3-triazole compound and provides guidance for using simple and high-selectivity  $\text{Hg}^{2+}$  probes in aqueous solutions under physiological conditions (pH 7.40).

Based on the favorable biological activity and chemical versatility of 1,2,3-triazoles, there is still a forever demand to exploit and utilize new 1,2,3-triazoles for highly selective and sensitive probing  $\text{Hg}^{2+}$  ions in actual samples. In present work, 5-methyl-1-phenyl -1*H*-1,2,3-triazole-4-carboxylic acid (MPC, Scheme 1) was a novel compound generated from copper-catalyzed oxidative reactions [47]. The structural properties for MPC such as electron affinity, ionization potential, molecular orbitals, and predicted spectra had been performed by TD-DFT method with HF/6-31G(d) and B3LYP/6-31G(d) basis set. Moreover MPC was designed and synthesized with rhodamine B to produce a new derivative called RMPC, which showed excellent selectivity to  $\text{Hg}^{2+}$  with colorimetric reaction over other metal ions.

## 2. Experimental section

### 2.1. Materials and instrumentation

MPC was provided by Organic Chemistry Laboratory of Hainan Normal University, China. The stock solution of MPC ( $5.0 \times 10^{-4}$  mol/L) was prepared in methanol. The tris buffer solution (pH 7.4) was selected to keep the pH values of the systems. Sodium hydroxide and chloride salts such as  $\text{Mg}^{2+}$ ,  $\text{Mn}^{2+}$ ,  $\text{K}^+$ ,  $\text{Na}^+$ ,  $\text{Co}^{2+}$ ,  $\text{Ca}^{2+}$ ,  $\text{Cd}^{2+}$ ,  $\text{Pb}^{2+}$ ,  $\text{Cu}^{2+}$ ,  $\text{Ni}^{2+}$ ,  $\text{Fe}^{3+}$ ,  $\text{Zn}^{2+}$ ,  $\text{Ag}^+$ ,  $\text{Hg}^{2+}$  and  $\text{Li}^+$  were purchased from Sinopharm Chemical Reagent Co., Ltd (Shanghai, China). All other reagents were of analytical reagent grade and obtained commercially without further purification. Doubly distilled water was used throughout the experiment.

NMR spectra were recorded on a Bruker Avance 400 MHz spectrometer at 400 MHz in  $\text{CDCl}_3$  at room temperature. Fluorometric experiments were performed on a RF-5301PC spectrofluorophotometer

(Shimadzu, Japan) and a F-7000 Spectro fluorophotometer (Hitachi, Japan) equipped with a xenon lamp source and a water bath. The UV-vis absorbance spectra were measured on a Hitachi U3900/3900H spectrophotometer (Hitachi, Japan) equipped with 1.0 cm quartz cells. ESI-MS spectra were recorded on an Agilent 1100-Bruker Esquire HCT at room temperature. The compound was ionized in the electrospray ionization (ESI) and operated in negative mode.

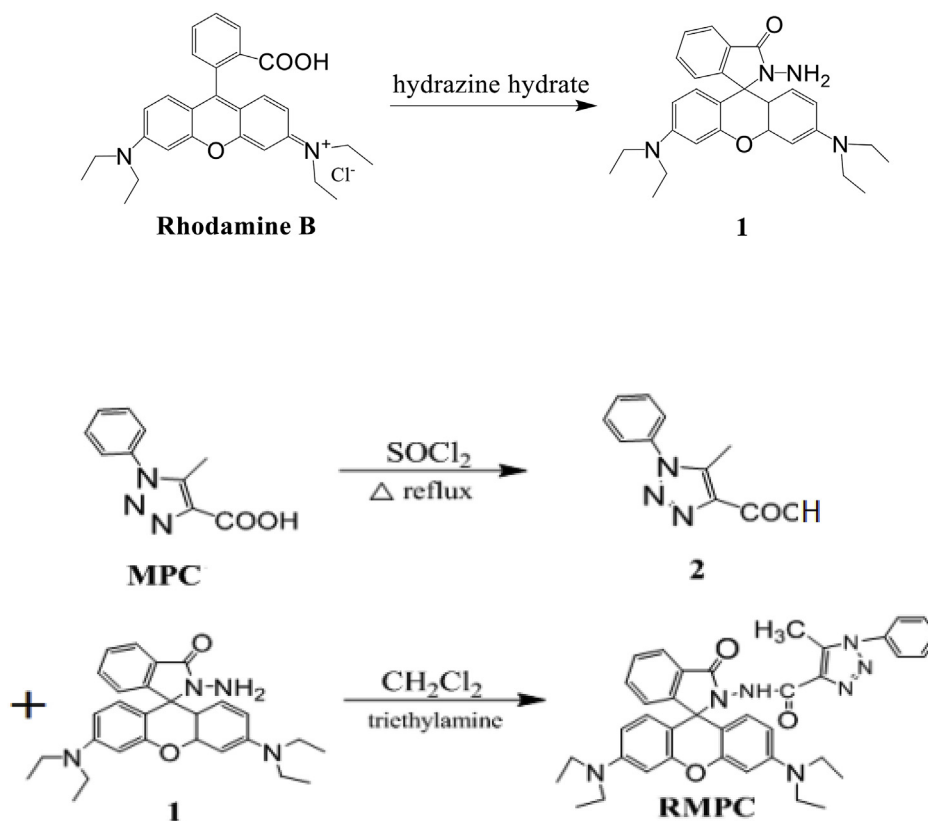
### 2.2. Synthesis

As shown in Scheme 1, the first step is to synthesize rhodamine B hydrazide (1) according to the reported reference [48]. Rhodamine B (1.0 g, 2.1 mmol) and 80% hydrazine hydrate (2 mL) were mixed and stirred in 20 mL ethanol at room temperature. Then the mixture was heated to reflux for 3 h and extracted with ethyl acetate (50 mL) for three times. The supernatant was dried over anhydrous sodium sulfate and filtered, obtaining intermediate 1 as a yellow solid (0.52 g, 54.74%);  $^1\text{H}$  NMR (400 MHz,  $\text{CDCl}_3$ ): $\delta$  (ppm) = 1.16 (t,  $J$  = 6.8 Hz, 12H), 3.34 (q,  $J$  = 7.2 Hz, 8H), 3.61 (s, 2H), 6.30 (m, 2H), 6.45 (m, 4H), 7.1 (m,  $J$  = 2.64 Hz, 1H), 7.44 (m, 2H), 7.94 (m, 1H);  $^{13}\text{C}$  NMR (400 MHz,  $\text{CDCl}_3$ )  $\delta$  (ppm) = 166.03, 153.75, 151.45, 148.78, 132.39, 129.91, 128.00, 127.95, 123.71, 122.83, 107.94, 104.47, 97.89, 77.32, 77.00, 76.68, 65.82, 44.25, 12.50.

The next step is to synthesize RMPC as follows: A mixture of MPC (100 mg, 0.49 mmol) and a solid of  $\text{SOCl}_2$  (2.3 mL) in a 10 ml round-bottomed flask was heated to reflux for 3 h. Then the distillation device substituted the reflux device and the residuary  $\text{SOCl}_2$  was distilled out. The product 2 was obtained and dissolved in 10 mL dichloromethane. Also it was mixed with rintermediate 1 (230 mg, 0.50 mmol) and 1 mL ethylenediamine. Then the mixture was stirred at room temperature for 12 h and extracted with  $\text{H}_2\text{O}$  and ethyl acetate. The organic phase was washed for three times with water and dried over  $\text{Na}_2\text{SO}_4$ . The solvent was removed by evaporation and the crude product was dried. After drying, the crude product was purified on a silica column using petroleum ether: ethyl acetate (2:1, v/v) as the eluent to afford product RMPC (130.2 mg, 41.21%).  $^1\text{H}$  NMR (400 MHz,  $\text{CDCl}_3$ )  $\delta$  8.40 (s, 1H), 7.98 (d,  $J$  = 6.4 Hz, 1H), 7.56–7.43 (m, 5H), 7.38–7.35 (m, 2H), 7.12 (d,  $J$  = 6.6 Hz, 1H), 6.78 (d,  $J$  = 8.5 Hz, 2H), 6.36 (s, 3H), 6.33 (s, 1H), 3.34 (q,  $J$  = 7.0 Hz, 8H), 2.49 (s, 3H), 1.16 (t,  $J$  = 7.0 Hz, 12H);  $^{13}\text{C}$  NMR (100 MHz,  $\text{CDCl}_3$ )  $\delta$  165.14, 158.87, 153.66, 152.36, 149.01, 137.82, 136.95, 135.51, 133.15, 129.98, 129.65, 129.26, 128.69, 128.16, 125.27, 124.03, 123.50, 108.17, 104.39, 97.89, 77.40, 77.08, 76.76, 66.04, 44.36, 12.68, 9.77. HRMS (ESI) ( $m/z$ ):  $[\text{M} + \text{H}]^+$  calcd for  $\text{C}_{38}\text{H}_{40}\text{N}_7\text{O}_3$ , 642.3193; found, 642.3199.

### 2.3. Computational study

All quantum chemical calculations were performed by using the GaussView5.0 program [49] in combined with Gaussian 09 software [50]. The molecular structures of MPC in the ground state were optimized by the GaussView5.0 program at Hartree-Fock Restricted algorithm level and the time-dependent density functional theory (TD DFT) including the CIS/6-31G(d) and B3LYP/6-31G(d) methods, respectively. The molecular orbital was analyzed using the HF/6-31G (d) method. The structural properties of MPC such as frontier molecular orbital LUMO, HOMO energies, and their band gap were calculated to exhibit the influence on the electron density transfer within the molecule. Moreover the values of electron affinity and ionization potential of MPC were carried out through DFT method at the DFT//B3LYP/6-31G\* basis set [50]. The predicted absorption spectra and fluorescence emission spectra of MPC were calculated by TD DFT method [49–51]. The configurations of the lowest excited state of MPC was fully optimized by the Configuration Interaction with Single excitations (CIS) method. Also, the molecular structure of the compound RMPTC was fully optimized by B3LYP method based on Gaussian 09 program package. Then the structural energy in terms of LANL2TZ basis set for



Scheme 1. The synthesis route of RMPC.

Hg and 6-311G(d) basis set for H, C, N, O, and F were calculated [52].

#### 2.4. Spectra measurements

The solutions of RMPC and Hg<sup>2+</sup> solutions of different concentration were prepared by stepwise dilution of a stock solution (0.5 mM for RMPC and 5 mM for Hg<sup>2+</sup>, respectively) in water and acetonitrile, respectively. The stock solution of RMPC (60 μL) was added into a quartz cell, then various metal ions of 50 μM were added respectively. The solution was diluted with DMF-water (v/v, 1:1, pH 7.4) to obtain a concentration of 10 μM for RMPC. The fluorescence and UV-vis absorption spectra titration were carried out by increasing the volume of different metal ions solution to a solution of RMPC. The excitation wavelength of the fluorescence experiment is set at 563 nm and that of emission wavelength at 584 nm, respectively. In order to evaluate the selectivity of RMPC for Hg<sup>2+</sup> detection, 16 kinds of competitive metal ions, including Pb<sup>2+</sup>, Mn<sup>2+</sup>, K<sup>+</sup>, Na<sup>+</sup>, Ag<sup>+</sup>, Ca<sup>2+</sup>, Cd<sup>2+</sup>, Co<sup>2+</sup>, Cu<sup>2+</sup>, Fe<sup>3+</sup>, Zn<sup>2+</sup>, Ni<sup>2+</sup>, Hg<sup>2+</sup>, Li<sup>+</sup> and Mg<sup>2+</sup> were measured under the same experimental condition with a final concentration of 40 μM. The fluorescence and UV-vis absorbance titrations were repeated for three times until the reasonable values were obtained.

#### 2.5. Cell culture and fluorescence imaging

HeLa cells were cultured on a 6-well plate with a density of  $2 \times 10^3$  cells per well in cell incubator at 37 °C with a humidified atmosphere for 12 h before staining. After removing culture media, cells were additionally washed with PBS buffer for three times. Then HeLa cells were incubated with chemosensor RMPC (10 μM) in the culture media containing ethanol for 30 min at 37 °C. The experiments to assess Hg<sup>2+</sup> uptake were performed in the same culture media supplemented with 25 μM Hg<sup>2+</sup> for 30 min. Moreover the fluorescence images were acquired through fluorescence microscopy.

### 3. Results and discussion

#### 3.1. Geometry optimization of MPC

The theoretical quantum chemistry methods based on HF and DFT are widely used for the calculation of optimized geometry, absorption spectrum, UV, IR, and NMR spectra of the organic molecules [53]. In the present work, the conformational analysis for the molecule MPC was performed to reach the most stable conformations. Then, the most stable conformations of MPC was fully optimized, and the corresponding quantum chemical calculations were obtained by using the GaussView5.0 program at Hartree-Fock Restricted algorithm level and the time-dependent density functional theory (TD DFT) including HF/6-31G(d) and B3LYP/6-31G(d) basis sets respectively (as shown in Fig. 1A). From Fig. 1A, it can be seen that the structure of MPC is nonplanar with various groups. The compound MPC contains 24 atoms, and the geometrical parameters of MPC including bond length and bond angle are listed in Table S1 by using HF/6-31G(d), CIS/6-31G(d), and B3LYP/6-31G(d) basis sets respectively. It is noticed that the calculated values of bond angles and bond lengths are semblable in all levels of calculations. The bond angle changed from 103.329 to 133.110°, and the bond length changed from 0.9497 Å to 1.4976 Å. However, the dihedrals appeared somewhat different because of different computing methods. Specifically, the C-C bond length in benzene ring is between 1.3544 and 1.4651 Å at three levels, which are much shorter than that of the classic C-C single bond (1.54 Å), shorter than that of the typical C-N bond (1.47 Å) and longer than that of the normal C=C double bond (1.34 Å) [54].

#### 3.2. Frontier molecular orbital analysis of MPC

Frontier molecular orbitals (FMO's) is one of the most useful and crucial tools to analyze the highest occupied molecular orbital (HOMO) and lowest unoccupied molecular orbital (LUMO) in quantum

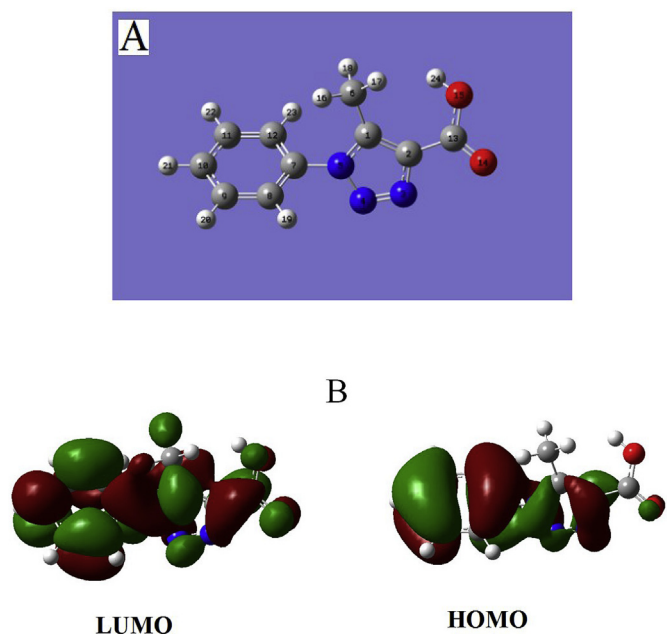


Fig. 1. (A) The optimized structure of MPC; (B1) The frontier molecular orbital of ground state on HOMO; (B2) The frontier molecular orbital of ground state on LOMO.

chemistry. Based on the FMO's theory, the interaction between HOMO and LUMO levels of the reacting subjects can lead to the formation of a transition state. Generally, LUMO can be thought as the innermost orbital containing free places and reflect the ability to accept an electron, while HOMO can be considered as the outermost orbital which contains electrons reflecting the ability to donate an electron. The lower energy of the LUMO means it is easier to accept electrons from some electron-donating groups. It is reported that the properties of HOMO have mainly impact on the ionization potential, and the properties of LUMO have directly impact on the electron affinity [55,56]. Fig. B1, and Fig. B2 exhibited the LUMO value of MPC (0.10848 eV) and the HOMO value of MPC (-0.35175 eV) respectively, which indicated that it is harder for MPC to accept electrons from other electron-donating group.

The energy difference between the LUMO and HOMO orbitals is named the energy gap, which acts as a crucial stability factor for the compound [57]. Herein the value of energy gap for MPC is 0.4602 eV, which indicated that the molecule has a stable structure but lower gap. A molecule with a small energy gap means more polarizable and is generally related to high chemical reactivity, low kinetic stability and is termed as soft molecule [58,59]. So it indicated that the electrons are more easily to be excited from the ground state to the excited state because of lower the energy gap, which is confirmed by the following results obtained from the spectral experiment. Additionally, the diffuse functions B3LYP/6-311G+(d) at the DFT//B3LYP/6-31G\* algorithm level were applied to calculate some physicochemical values such as adiabatic electron affinity (1.65 eV), vertical electron affinities (1.27 eV), adiabatic ionization potential (6.69 eV) and vertical ionization potential (7.07 eV). The obtained parameters implied that the electron accepting ability of MPC is very weak [60].

### 3.3. Spectral characterization of MPC

According to the FMO's theory, the LUMO-HOMO gap is also an important factor related to the luminescent properties [57,61]. The computed results on the energy difference between the LUMO and HOMO orbitals showed that the electron transition of MPC focused mainly on HOMO→LUMO transition. It indicated that MPC had optical properties, which was proved in the following experimental results.

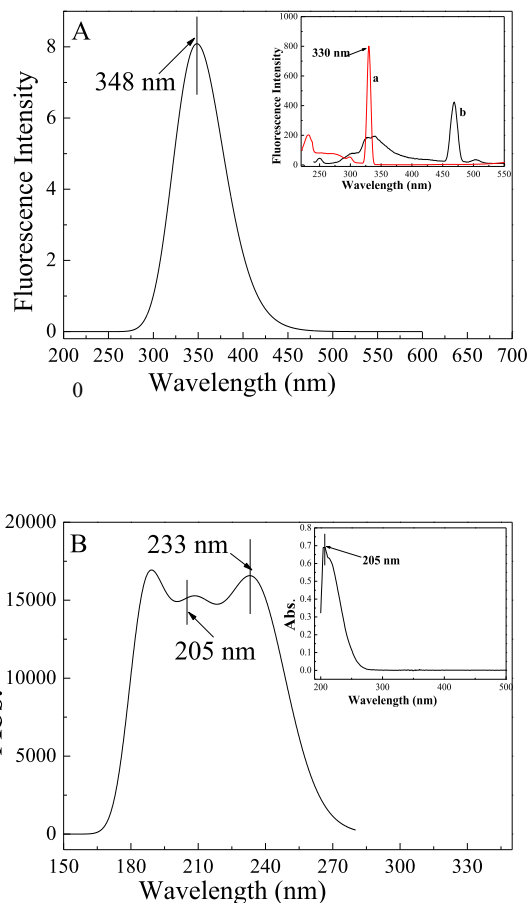


Fig. 2. (A) The calculated fluorescence emission spectra of MPC. inset: (a) the experimental fluorescence emission spectra of MPC (60  $\mu$ M) in methanol; (b) the experimental fluorescence excitation spectra of MPC (60  $\mu$ M) in methanol. (B) The calculated absorption spectra of MPC, inset: the experimental absorption spectra of MPC (60  $\mu$ M) in methanol.

Fig. 2A exhibited the emission spectra calculated by TD DFT methods and that of measured in methanol (plot "a" in the illustration of Fig. 2A). The calculated spectra displayed the maximum fluorescence emission peak at 348 nm, which is different from the experimental spectra measured at 330 nm in the plot "a" of Fig. 2A (inset). The rational explanation is that the conjugated aromatic compound MPC led to a  $\pi \rightarrow \pi^*$  transition from the ground state to an excited state. Owing to the solvent effect, the polarity of the ground state is weaker than that of excited state, and a stronger polar solvent can have more influence on stabilizing the excited state, which results in the position of maximum fluorescence emission peak shifting towards the shorter wavelength side [62]. Therefore, methanol, as a higher polar solvent, brought about the blue-shift effect with the shift of the maximum peak of fluorescence emission from 348 nm to 330 nm.

The computed electronic absorption spectra of MPC is shown in Fig. 2B, in which the illustration is the absorption spectra of MPC obtained from the experimental measurement in methanol. From Fig. 2B, it showed that both of the two graphs showed the distinguishing profiles with a broad peak for the computed spectra and a single peak for the measured spectra. The range of maximum absorption bands for the computed spectra is from 189 nm to 233 nm, and that of the measured spectra is only at 205 nm. In theory, the absorption peak at about 203 nm was attributed to E absorption band of  $\pi \rightarrow \pi^*$  transition, which is a typical spectral signal for aromatic compounds [63]. However, it is noticed that the maximum absorption peak is at 205 nm for the measured spectra, which is in good agreement within the range of the strong absorption peak obtained from the predicted spectra of MPC.

Based on the above fluorescence and absorption spectral analysis, the theoretically calculated results by DFT method are consistent with the experimental results in a great degree. According to the relevant absorption theory, the molar absorption coefficient ( $\epsilon = 2.126 \times 10^5 \text{ L/mol/cm}$ ) of MPC was determined from the plot of concentration vs. absorbance (Fig. S1 in Supplemental Materials). Due to the special structure of MPC, it is predicted that MPC should have higher fluorescence quantum efficiency because of its fluorescent emission peak at 330 nm and is a prospective blue light emitting fluorescent material in the organic light-emitting diodes [64].

### 3.4. Synthesis of RMPC

Many studies reported that the triazole motifs as the platform had been used to design and develop some new fluorescence chemosensors. Several highly selective chemosensors for the detection of various metal ions (such as  $\text{Zn}^{2+}$ ,  $\text{Cu}^{2+}$ ,  $\text{Fe}^{3+}$ ,  $\text{Cd}^{2+}$ , and  $\text{Hg}^{2+}$  etc.) based on click generated triazole have been synthesized and applied in different fields [65–68]. In the present study, it is possible and feasible for MPC to synthesize with rhodamine B hydrazide in principle due to the triazole structure containing ester group [69]. By improving the experimental conditions, a new rhodamine B derivative RMPC was synthesized by the reaction between MPC and the rhodamine hydrazide (Scheme 1). The structural characterizations of RMPC, including  $^1\text{H}$ NMR,  $^{13}\text{C}$  NMR, and HRMS, were shown in Fig. S2, Fig. S3, and Fig. S4 respectively in Supplemental Materials. The results can provide reasonable guidance for a synthetic reaction between similar compounds containing 1,2,3-triazole unit and rhodamine B.

### 3.5. Optimization of detection conditions

The selective recognition ability of RMPC for  $\text{Hg}^{2+}$  ions in various solutions with different pH value was performed. The effect of pH on the fluorescence intensity was measured between 3.0 and 10.0 for RMPC (10  $\mu\text{M}$ , plot “a”) and for RMPC- $\text{Hg}^{2+}$  system with a concentration of  $\text{Hg}^{2+}$  fixed at 50  $\mu\text{M}$  (plot “b”) in Fig. S5, respectively. From Fig. S5, it can be seen that RMPC showed remarkable fluorescence when the pH value is less than 4, illustrating that RMPC was a sensitive acid-responsive probe. While there was not any distinct and specific fluorescence for RMPC in the pH range from 4.0 to 10.0, which suggested the formation of stable spirocyclic RMPC complex in the range of the pH value. For RMPC- $\text{Hg}^{2+}$  complex, the fluorescence intensity was increased under the different pH value between 3.0 and 8.0, which implied that the complex maintained in a “turn-on” state in this pH range. However, it is very interesting to notice that the maximum fluorescence response to  $\text{Hg}^{2+}$  was found at the pH value as 7.4. If the pH value is higher than 7.4, there was no obvious fluorescence enhancement for RMPC. The rational explanation is that the metal ions might bind to the  $\text{OH}^-$  and form partial metal ion precipitation, which might decrease the actual concentration of metal ions in the sample solution and cause the decrease of fluorescence intensity. Taking the optimized pH condition into consideration, the fluorescence and UV–vis spectroscopic studies on RMPC and corresponding metal complexes were evaluated in pH 7.4, which also indicated that RMPC was suitable for detecting under physiological condition.

The effect of response time in the present system was measured, and the results were shown in Fig. S6. It can be seen that the fluorescence intensity of the RMPC- $\text{Hg}^{2+}$  system at 584 nm gradually enhanced less than 3 min and a plateau of fluorescence enhancement was achieved within 60min, which suggested that RMPC reacted with  $\text{Hg}^{2+}$  was fast and the reaction completed within 3min. Thus the proper response time is 3 min which can be applied in the related spectroscopic measures. Moreover RMPC could be used for the real-time detection of  $\text{Hg}^{2+}$  in aqueous samples.

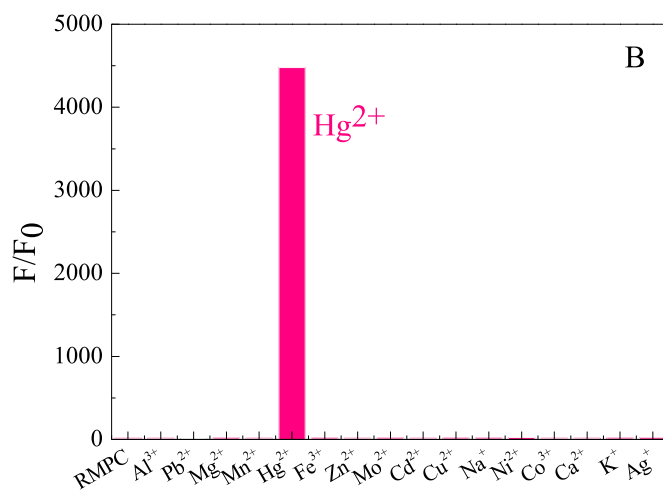
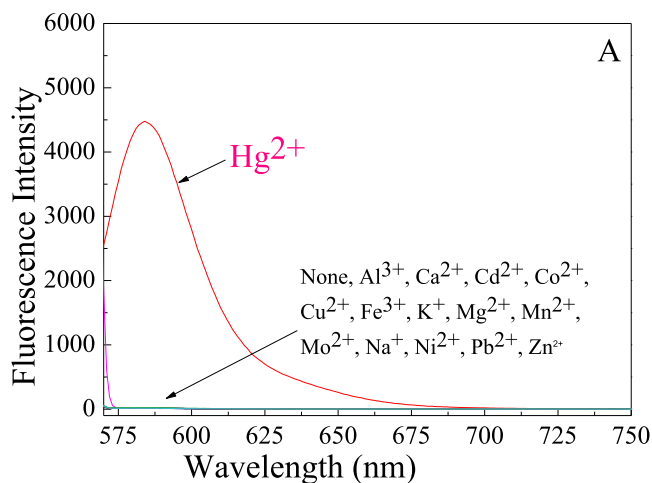
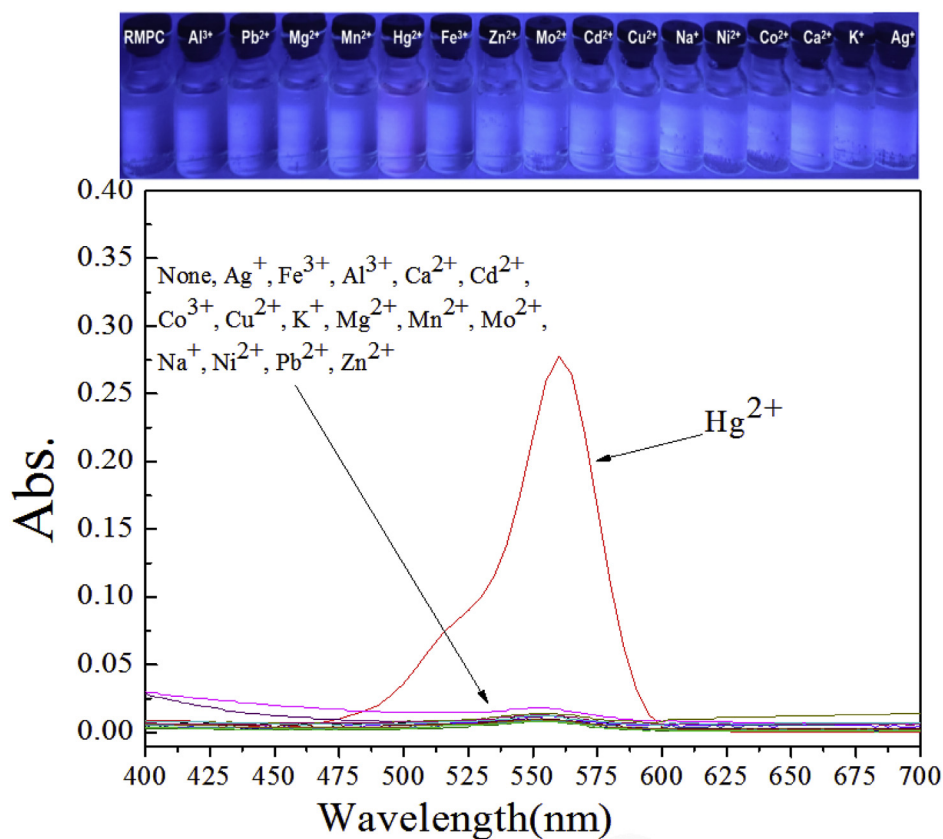


Fig. 3. The fluorescence spectra (A) and fluorescence intensities (B) at 584 nm of RMPC (50  $\mu\text{M}$ ) in DMF-water ( $v/v = 1/1$ , Tris-HCl, pH 7.4) in the presence of various cations (40  $\mu\text{M}$ ) ( $\lambda_{\text{ex}} = 563 \text{ nm}$ ).

### 3.6. Fluorescence and UV–vis spectra of the interaction of RMPC with $\text{Hg}^{2+}$

The binding behavior of RMPC towards various metal ions ( $\text{Pb}^{2+}$ ,  $\text{Mn}^{2+}$ ,  $\text{K}^+$ ,  $\text{Na}^+$ ,  $\text{Ag}^+$ ,  $\text{Ca}^{2+}$ ,  $\text{Cd}^{2+}$ ,  $\text{Co}^{2+}$ ,  $\text{Cu}^{2+}$ ,  $\text{Fe}^{3+}$ ,  $\text{Zn}^{2+}$ ,  $\text{Ni}^{2+}$ ,  $\text{Hg}^{2+}$ ,  $\text{Li}^+$  and  $\text{Mg}^{2+}$ ) was studied by fluorescence and UV–vis spectroscopy in DMF/ $\text{H}_2\text{O}$  ( $v/v = 1:1$ , Tris-HCl, pH = 7.4) solutions. Fig. 3A displayed the changes on the fluorescence spectra for RMPC in the presence and absence of various metal ions. Free RMPC (50  $\mu\text{M}$ ) solution is colorless and nonfluorescent, which indicated the rhodamine moiety in ring-closed spirolactam form. Upon the addition of  $\text{Hg}^{2+}$  ion (40  $\mu\text{M}$ ), a fluorescence emission band at 584 nm with excitation at 563 nm was observed, which further suggested ring-opened RMPC- $\text{Hg}^{2+}$  complex was generated. Besides that, the fluorescence emission band almost had no changes while other metal ions were added at the same condition. As shown the appended drawings in Fig. 3B, it exhibited the photographs of the RMPC in the presence of all testing metal ions. Correspondingly, it is only  $\text{Hg}^{2+}$  ion that changed the fluorescence intensity and the color of RMPC solution from colorless to pink compared to other metal ions. There were not any significant color and spectral change under identical conditions in the presence of other metal ions. Generally, rhodamine spirolactam derivatives are colorless and nonfluorescent, whereas ring-opening of the relevant spirolactam can cause stronger fluorescence emission and a pink color observed [69]. The selectivity of RMPC to  $\text{Hg}^{2+}$  over other metal ions was



**Fig. 4.** The absorption spectra of RMPC (50  $\mu\text{M}$ ) in the presence of different metal ions (40  $\mu\text{M}$ ) in DMF-water ( $v/v = 1/1$ , Tris-HCl, pH 7.4). Inset: The photographs of the RMPC in the presence of  $\text{Hg}^{2+}$  and other metal ions under ultraviolet light.

measured by the fluorescence experiments (Fig. 3(B)). It can be seen that the addition of  $\text{Hg}^{2+}$  to RMPC solution led to a 4500-fold increase in fluorescence intensity at 584 nm. The result indicated that RMPC could act as a sensor to detect  $\text{Hg}^{2+}$  through their distinct fluorescence “off-on” responses by the naked eye. Moreover it is likely to form a novel compound between RMPC and  $\text{Hg}^{2+}$  due to ring-opening from the spirolactam (RMPC) to ring-opened amide (RMPC- $\text{Hg}^{2+}$  system). So it is demonstrated that the developed colorimetric sensor possesses high selectivity for  $\text{Hg}^{2+}$  sensing, which may be due to the unique interaction between RMPC and  $\text{Hg}^{2+}$ .

Fig. 4 is the UV-vis spectroscopy of RMPC in the absence and presence of different metal ions measured in DMF- $\text{H}_2\text{O}$  ( $v/v = 1:1$ , Tris-HCl, pH 7.40). It is noticed that there was a new absorption band at 565 nm for RMPC- $\text{Hg}^{2+}$  complex with the increasing absorption intensity. Other tested metal ions (such as  $\text{Pb}^{2+}$ ,  $\text{Mn}^{2+}$ ,  $\text{K}^+$ ,  $\text{Na}^+$ ,  $\text{Ca}^{2+}$ ,  $\text{Cd}^{2+}$ ,  $\text{Co}^{2+}$ ,  $\text{Cu}^{2+}$ ,  $\text{Fe}^{3+}$ ,  $\text{Zn}^{2+}$ ,  $\text{Ni}^{2+}$ ,  $\text{Li}^+$  and  $\text{Mg}^{2+}$  ions) did not exhibit any new band formed under the same experimental conditions. Similarly, the formation of RMPC- $\text{Hg}^{2+}$  complex also brings about the color change of the solution, as the same as shown in the photographs of Fig. 4. The above results suggested that RMPC could be developed for the noticeable naked-eye detection of  $\text{Hg}^{2+}$  ions, accompanied by an obvious pink color appearing. The changes in color formation could be explained by the metal-induced delactonization of rhodamine. Upon RMPC binding with  $\text{Hg}^{2+}$  ions, colorless spirolactam form is turned into its colored ring-opened amide form.

### 3.7. Sensitivity of RMPC to $\text{Hg}^{2+}$ ions

The fluorescence and UV-vis titration measurements for RMPC with the progressive addition of  $\text{Hg}^{2+}$  ions were carried out, as shown in Fig. 5. The fluorescence intensity of RMPC (10  $\mu\text{M}$ ) at 584 nm was gradually enhanced with the increasing concentration of  $\text{Hg}^{2+}$  ions and

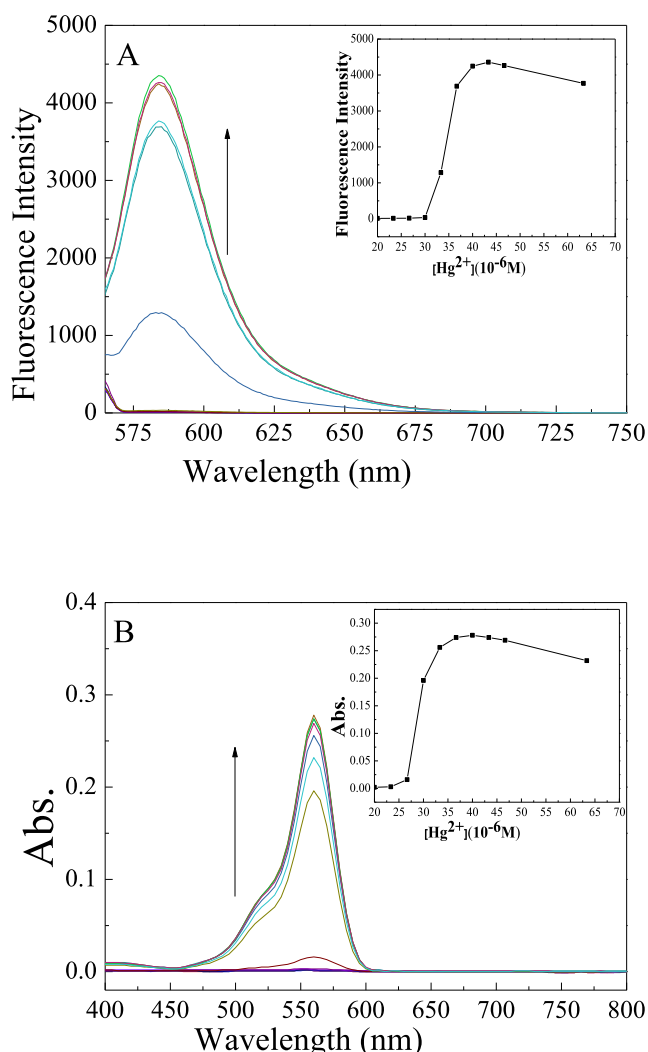
consequently became saturated when the concentration of  $\text{Hg}^{2+}$  reached 40  $\mu\text{M}$  (Fig. 5A). The linear plot for fluorescence enhancement of RMPC in the presence of  $\text{Hg}^{2+}$  was drawn in the range of  $2.67 \times 10^{-5}$ – $4.33 \times 10^{-5}$  M ( $R^2 = 0.9511$ , Fig. S7 in Supplemental Materials).

Fig. 5B showed the spectral changes of RMPC upon the gradual addition of  $\text{Hg}^{2+}$  by the UV-vis titration experiments. An absorption band centered at 565 nm appeared and gradually increased with the successive increase of  $\text{Hg}^{2+}$  ion concentration. When the amount of  $\text{Hg}^{2+}$  was increased from  $2.33 \times 10^{-5}$  to  $3.67 \times 10^{-5}$  M, the absorption intensity at 565 nm gradually enhanced. However, the observed attainment of the plateau (the illustration in Fig. 5B) suggested saturation in the interaction between the compound RMPC with the addition of  $\text{Hg}^{2+}$ . A linear relationship was observed between the absorbance and the concentration of  $\text{Hg}^{2+}$  ions with a correlation coefficient of  $R^2 = 0.9463$  (Fig. S8).

The above results from the fluorescence and UV-vis titration measurements demonstrated that the dynamic response range is too narrow. We think the most plausible reason is due to the triazole structure of RMPC only containing an ester group, which led to a less than ideal response ranges and detection limit. It is indicated that RMPC was potentially applicable for qualitative analysis rather than quantitative analysis of  $\text{Hg}^{2+}$  ion under physiological conditions (pH 7.40). Some other researches using biomolecular instead of organic molecular as a probe showed better dynamic response ranges and detection limit [70,71]. We will make attempts to use some biomolecular materials instead of organic molecular as a biosensor for facile detection of metal ions in further research.

### 3.8. The binding stoichiometry of RMPC and $\text{Hg}^{2+}$ complex

Several studies showed that rhodamine B and triazoles appended



**Fig. 5.** (A) The fluorescence spectrum of RMPC (10  $\mu\text{M}$ ) in DMF-H<sub>2</sub>O ( $v/v = 1/1$ , Tris-HCl, pH 7.4) upon increasing concentration of Hg<sup>2+</sup> ions ( $2.67 \times 10^{-5}$ – $4.33 \times 10^{-5}\text{M}$ ) ( $\lambda_{\text{ex}} = 563 \text{ nm}$ ,  $\lambda_{\text{em}} = 584 \text{ nm}$ ), inset: The plot of fluorescence intensity versus concentration of Hg<sup>2+</sup> ions. (B) The absorption spectral changes of RMPC (50  $\mu\text{M}$ ) at increasing concentrations of Hg<sup>2+</sup> ( $2.33 \times 10^{-5}$ – $3.67 \times 10^{-5}\text{M}$ ), inset: The plot of absorption intensity against the concentration of Hg<sup>2+</sup> ions.

derivatives can bond with various metal ions by displaying a particular color and the different complex ratio [58,66]. A plot of the fluorescence intensity versus the molecular fraction of  $[\text{RMPC}]/([\text{RMPC}] + [\text{Hg}^{2+}])$  was provided in Fig. 6A by using the equimolar continuous variations method [72]. The working curve showed that maximum emission intensity was measured for a molar fraction of ca. 0.33, indicating the binding stoichiometry between RMPC and Hg<sup>2+</sup> was 1:2. This result was also confirmed by quantum-chemistry calculation as follows. Firstly, both molecular structures of complexes on RMPTC binding to one and two Hg<sup>2+</sup> ions were fully optimized, respectively. Then their structural energies were determined by using B3LYP procedure in terms of LANL2TZ basis set for Hg and 6-311G(d) basis set for H, N, C, F, and O respectively. The calculated results were listed in Table 1 and Fig. 6B. From Table 1, it can be seen that the formation of RMPC-Hg<sup>2+</sup> complex as 1:2 stoichiometry generated the energy difference of  $\Delta E(\text{eV})$  and  $\Delta E(\text{a.u.})$ , which were smaller than that of as 1:1 stoichiometry. The values of bond length for Hg–O in RMPC-Hg<sup>2+</sup> complex as 1:2 stoichiometry was shorter than that of as 1:1 stoichiometry. The values of Mayer bond order for Hg–O in RMPC-Hg<sup>2+</sup> complex as 1:2 stoichiometry was higher than that of as 1:1 stoichiometry. These results indicated that the

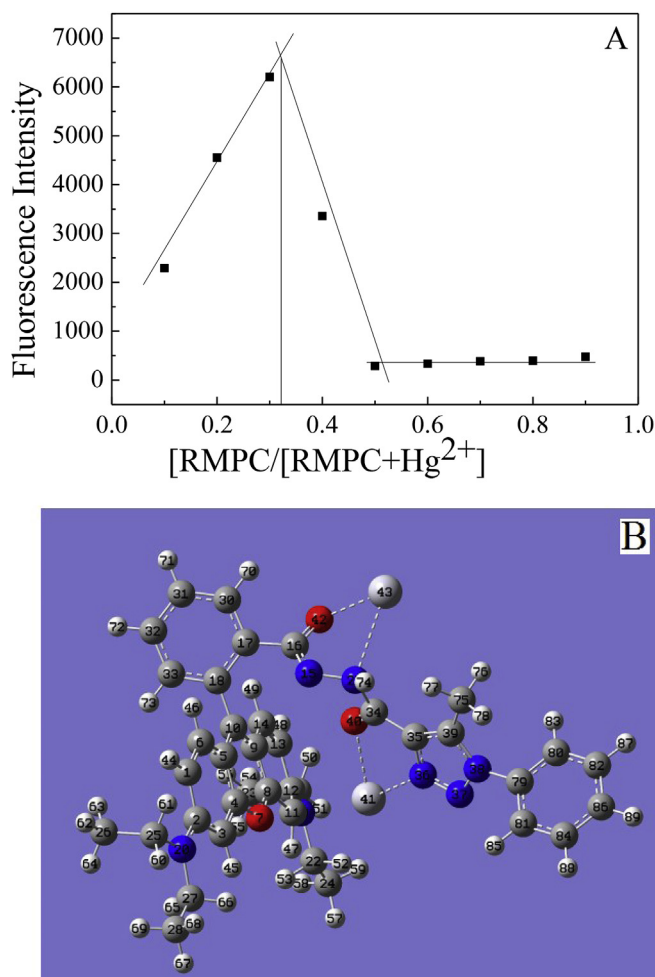


**Fig. 6.** (A) The working curve for determining the stoichiometry of RMPC and Hg<sup>2+</sup>. (B) The optimized structure of RMPC binding to two of Hg<sup>2+</sup> ions.

formation of RMPC-Hg<sup>2+</sup> complex as 1:2 stoichiometry was more rational and stable, which was verified theoretically in the following experimental result. Fig. 6B depicted a reasonable structure of RMPTC-Hg<sup>2+</sup> complex as 1:2 stoichiometry, and the corresponding parameters were showed in Table S2. As shown in Fig. 6B, the molecule of RMPC seems like as two pairs of tongs, one pair of them is formed between one Hg<sup>2+</sup> ion and one nitrogen atom and oxygen atom from hydrazide unit, another pair came from the ligand between another Hg<sup>2+</sup> ion and one nitrogen atom from triazoles group and one oxygen atoms from carbonyl group, respectively. The molecular modeling demonstrated that RMPC could provide proper space to hold two Hg<sup>2+</sup> ions with two penta cyclic groups formed.

### 3.9. Selectivity of RMPC to Hg<sup>2+</sup> ions

In order to prove that RMPC was highly selective for Hg<sup>2+</sup>, the competition experiments were carried out in the presence of Hg<sup>2+</sup> (10  $\mu\text{M}$ ) mixed with the other metal ion (50  $\mu\text{M}$ ) at the same experimental conditions (as shown Fig. 7). From Fig. 7, it can be seen that there had not obvious influence on the fluorescence intensity of RMPC-Hg<sup>2+</sup> system by the coexistence of other tested metal ions at this concentration. Correspondingly, it is only Hg<sup>2+</sup> ions that generated the fluorescence turn-on responses, and all the measured coexistent metal ions had no notable changes on the fluorescence intensity. The results showed that these competitive metal ions have no interference on Hg<sup>2+</sup> determination, suggesting RMPC can be applied to detect Hg<sup>2+</sup> effectively.

**Table 1**  
Comparison on energy changes of RMPC binding to  $\text{Hg}^{2+}$  using the B3LYP functional in Gaussian 09.

RMPC: $\text{Hg}^{2+}$	Energy change				
	$E_{\text{RMPC}}(\text{a.u.})$	$E_{\text{Hg}^{2+}}(\text{a.u.})$	$E_{\text{RMPC:Hg}^{2+}}(\text{a.u.})$	$\Delta E(\text{a.u.})$	$\Delta E(\text{ev})$
1:1	-2080.90	-41.79	-2123.14	-0.44	-12.02
1:2	-2080.90	-83.59	-2164.98	-0.49	-13.42

Bond length (Å)					
1:1	Hg-O	Hg(88)-O(29) 2.46		Hg(88)-O(41) 2.62	
	Hg-N	/		/	
1:2	Hg-O	Hg(43)-O(42) 2.31		Hg(41)-O(40) 2.52	
	Hg-N	Hg(43)-N(29) 2.91		Hg(41)-N(36) 2.36	

Mayer bond order					
1:1	Hg-O	Hg(88)-O(29) 0.26		Hg(88)-O(41) 0.17	
	Hg-N	/		/	
1:2	Hg-O	Hg(43)-O(42) 0.46		Hg(41)-O(40) 0.18	
	Hg-N	Hg(43)-N(29) 0.16		Hg(41)-N(36) 0.30	

### 3.10. Proposed mechanism of RMPC response to $\text{Hg}^{2+}$

Based on the above fluorescence, UV-visible spectral analysis, and working curve, the proposed mechanism of detecting  $\text{Hg}^{2+}$  was shown in Scheme 2. The compound RMPC is colorless and nonfluorescent, which indicated the characteristic closed ring state for rhodamine B domain due to the link to MPC. The addition of  $\text{Hg}^{2+}$  made the spirocycle open via coordination with one molecule of RMP binding to two molecules of  $\text{Hg}^{2+}$ . It also exhibited that an obvious color change from the colorless to pink associated with the reaction of RMPC with  $\text{Hg}^{2+}$  is readily detectable visually, while no significant color changes are promoted by other metal ions. So RMPC is high selectivity for the qualitative detection of  $\text{Hg}^{2+}$  ions. This binding mode is also consistent with the fluorescence enhancement changes observed as the induced conformational changes of the triazole groups RMPC upon 1:2 complexation, which was confirmed by ESI-MS measurement (Fig. 8A). As shown in Fig. 8A, there is the strongest peak at  $m/z$  902.4, which is likely to assign to  $[\text{RMPC} + \text{Hg} + \text{Na} + \text{Cl} + 2\text{H}]$  with less feasibility. However, a peak at  $m/z$  1066.3 has stronger intensity, which appears to

be more rational and can be assigned to  $[\text{RMPC} + 2\text{Hg} + \text{Na}]$ . The calculated isotopic patterns (Fig. 8A, inset) matches those measured fairly well.

In principle, to design a satisfactory fluorescence sensor systems (the host) for probing small molecules (the guest), it is crucial to utilize typical chemical reactions or host-guest interactions that lead to a change in the optical characteristic of the system. If the binding of the host to the guest is reversible and noncovalent, and the reaction can be interrupted under certain conditions, the indicator is called as a chemosensor [73–75]. Many studies related to the fluorescent chemosensors based on spiraling-opening reactions of rhodamine have been reported in recent years [51,65,66,69]. If the interaction mode between the guest and the host is based on an irreversible chemical reaction, the indicator is referred to as a chemodosimeter. In view of chemodosimeters, it is important that there are at least two functional groups. One of two groups is the reaction region, in which the host interacts with the detection object. Moreover another group is responsible for a spectral signal that relies on the reacting to the analyte. Both the interaction between the detection object and the analyte and the alteration of the

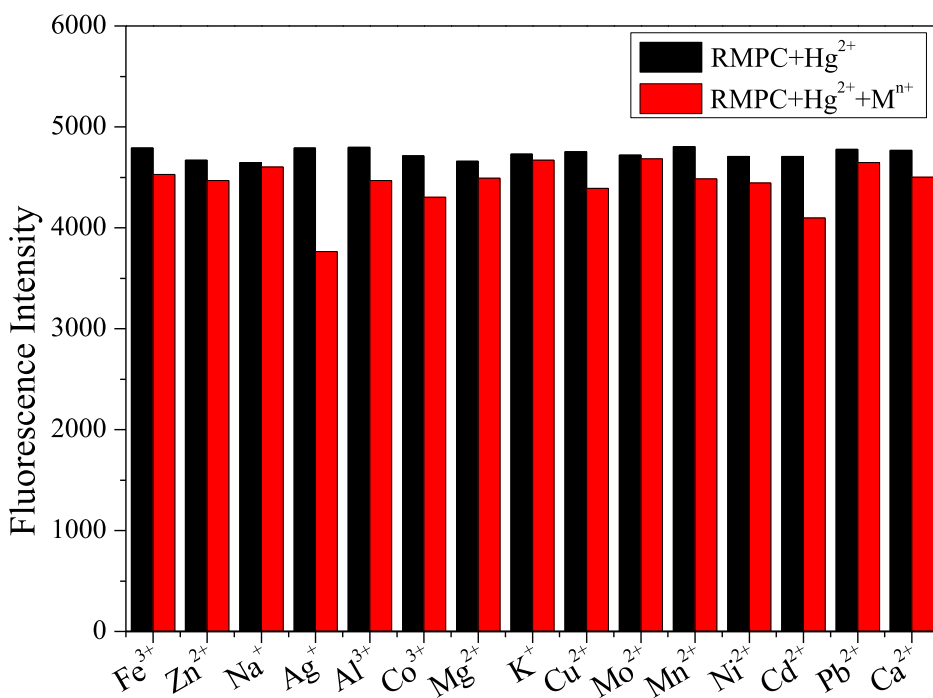
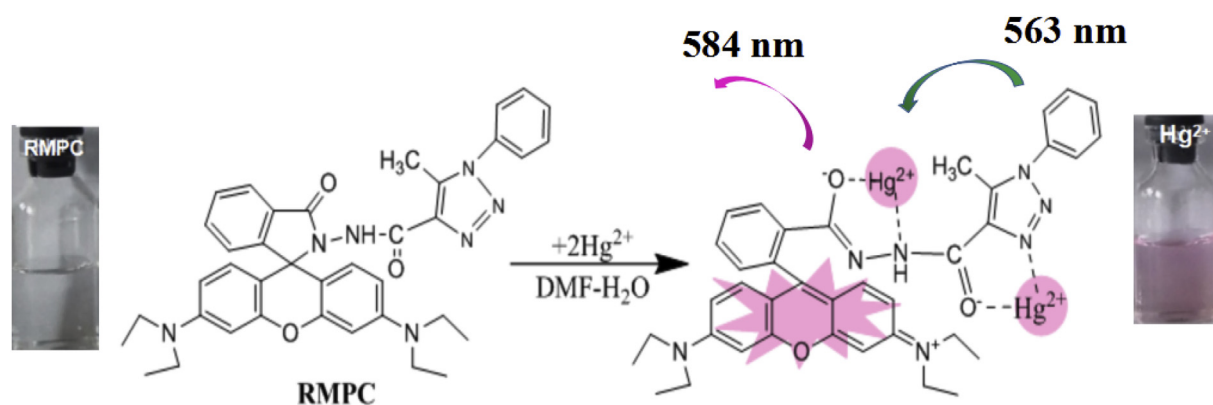


**Fig. 7.** The fluorescent change of RMPC (50  $\mu\text{M}$ ) toward  $\text{Hg}^{2+}$  over various competitive metal ions (5.0  $\mu\text{M}$ ) in DMF-water ( $v/v = 1/1$ , Tris-HCl, pH7.40).  $\lambda_{\text{ex}} = 563 \text{ nm}$ ,  $\lambda_{\text{em}} = 584 \text{ nm}$ . The black bars represent the intensity of the solution upon the addition of  $\text{Hg}^{2+}$  (50  $\mu\text{M}$ ). The red bars represent the intensity of RMPC in the presence of other metal ions (50  $\mu\text{M}$ ) and  $\text{Hg}^{2+}$  (50  $\mu\text{M}$ ). (For interpretation of the references to color in this figure legend, the reader is referred to the Web version of this article.)



Scheme 2. The proposed recognition mechanism of RMPC towards  $\text{Hg}^{2+}$ .

detection signal are irreversible [74]. In general, rhodamine derivative exhibits a red color variation and distinct fluorescence in acidic solutions by activating a carbonyl group in a spirolactam or spironolactone unit. Similarly, a proper ligand on a spironolactone ring can cause a color change as well as a fluorescence change in the presence of some metal ions, even though the extent of this reaction depended on the chosen solvent system [69]. In the present work, the binding of RMPC to  $\text{Hg}^{2+}$  could induce the formation of the ring-opened state of RMPC from the spirolactam state. Therefore RMPC would act as a “naked-eye” chemodosimeter targeted to  $\text{Hg}^{2+}$ , similar to some researches on rhodamine-appended fluorescence indicator for specific detection of metal ions [76–78].

### 3.11. Determination of $\text{Hg}^{2+}$ in HeLa cell

Based on the above, it indicated that a color change from the colorless to pink associated with the reaction of RMPC with  $\text{Hg}^{2+}$  is readily detectable visually. In order to examine the practical properties of RMPC in biological samples, the probe was applied for detecting  $\text{Hg}^{2+}$  in HeLa cell by fluorescence microscopy. As depicted in Fig. 9, a bright-field transmission image of cells with  $\text{Hg}^{2+}$  and RMPC confirmed that the cells were viable throughout the imaging experiments, implying the probe RMPC can penetrate the cell membrane and image  $\text{Hg}^{2+}$  ions in HeLa cells, with the switching-on fluorescent signal.

## 4. Conclusion

In summary, a novel 1,2,3-triazoles compound, 5-methyl-1-phenyl-1H-1,2,3-triazole-4-carboxylic acid (MPC), was studied on the structural feature, theoretical and experimental spectral characteristic by quantum chemistry and spectroscopic methods, respectively. The measured results are consistent with those theoretical calculations derived from structural parameters, which guided for making full use of MPC in the photophysical field due to its typical spectral property. Then a new fluorescent chemodosimeter based on rhodamine derivative RMPC for the detection of  $\text{Hg}^{2+}$  was synthesized. The probe displayed high selectivity for  $\text{Hg}^{2+}$  over other metal ions in DMF- $\text{H}_2\text{O}$  (v/v = 1/1, pH 7.4) solutions with color changes facilitating “naked-eye” recognition for  $\text{Hg}^{2+}$ . While the 1:2 stoichiometry of the complex formed between chemodosimeter RMPTC and  $\text{Hg}^{2+}$  showed the potential for quantitative determination of  $\text{Hg}^{2+}$  ions. The fluorescence imaging of  $\text{Hg}^{2+}$  in HeLa cells was successfully operated, demonstrating that RMPC is of good membrane-permeable reagent for the biological imaging applications.

## Declaration of competing interest

The authors have declared no conflict of interest.

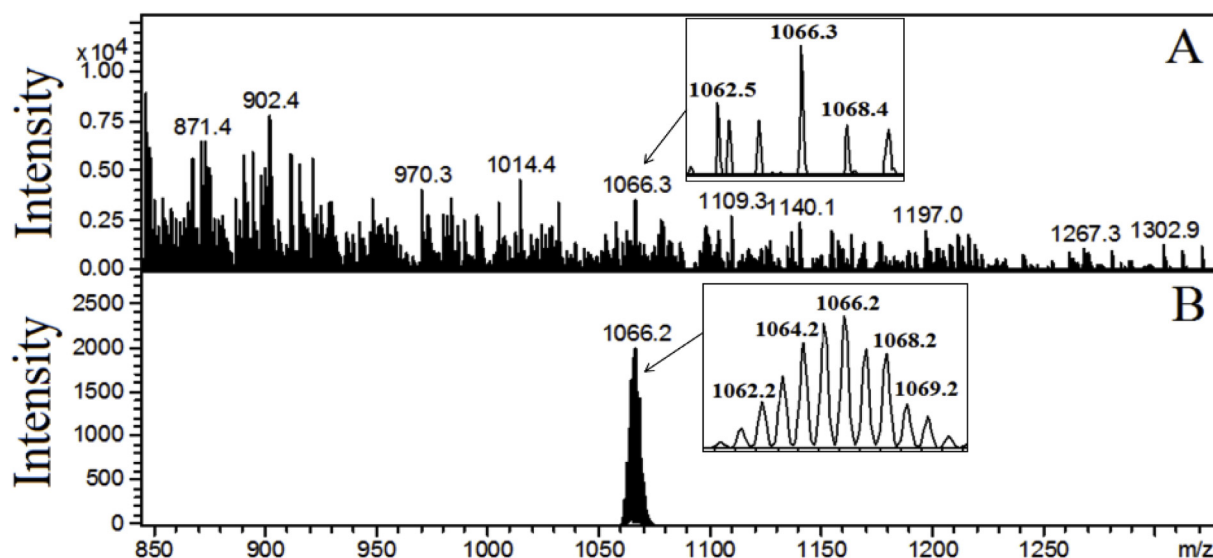


Fig. 8. (A) ESI-MS of RMPC in the presence of  $\text{Hg}^{2+}$  and trace amounts of  $\text{Cl}^-$ . Inset: enlarged patterns for the  $[\text{RMPC} + 2\text{Hg} + \text{Na}]$ . (B) The calculated ESI-MS of RMPC in the presence of  $\text{Hg}^{2+}$  and  $\text{Cl}^-$ . Inset: calculated isotopic patterns for the  $[\text{RMPC} + 2\text{Hg} + \text{Na}]$ .

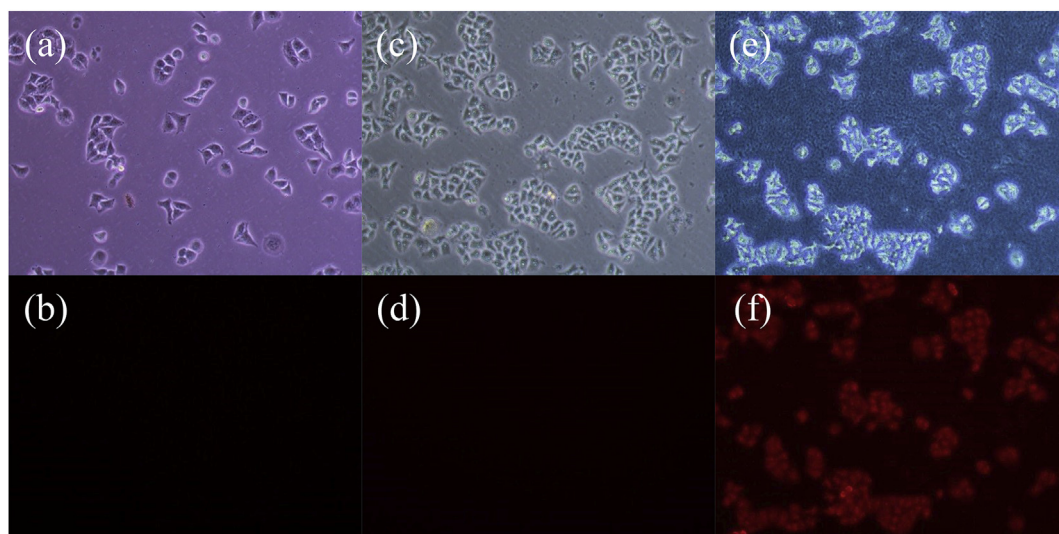


Fig. 9. The fluorescence imaging of  $\text{Hg}^{2+}$  in HeLa cell with RMPC.

(a, c, e) The brightfield transmission images; (b) The images of cells incubated with the FBS culture solution as the sample blank; (d) The images of cells incubated with RMPC (10  $\mu\text{M}$ ); (f) The images of cells incubated with RMPC (10  $\mu\text{M}$ ) and  $\text{Hg}^{2+}$  (20  $\mu\text{M}$ ).

## Acknowledgments

Funding for this work is provided by National Natural Science Foundation of China (No. 21562019); Natural Science Foundation of Hainan Province (No. 219MS040); Hainan province natural science foundation of innovative research team project (2016CXTD007).

## Appendix A. Supplementary data

Supplementary data to this article can be found online at <https://doi.org/10.1016/j.ab.2020.113690>.

## References

- J.P. Zhu, K.Y. Li, C.Y. Zhang, J.F. Wang, S.J. Chen, Preparation, crystal structure, thermal behaviors and DFT studies of 4,4,5,5-tetraacetamine-3,30-bi(1,2,4-triazole), *J. Mol. Struct.* 1145 (2017) 285–291, <https://doi.org/10.1016/j.molstruc.2017.05.106>.
- J. Totobenazara, A.J. Burke, New click-chemistry methods for 1, 2, 3-triazoles synthesis: recent advances and applications, *Tetrahedron Lett.* 56 (2015) 2853–2859, <https://doi.org/10.1016/j.tetlet.2015.03.136>.
- N.N. Fu, S.L. Wang, Y.Q. Zhang, C.X. Zhang, D.L. Yang, L.X. Weng, B.M. Zhao, L.H. Wang, Efficient click chemistry towards fatty acids containing 1,2,3-triazole: design and synthesis as potential antifungal drugs for *Candida albicans*, *Eur. J. Med. Chem.* 136 (2017) 596–602, <https://doi.org/10.1016/j.ejmech.2017.05.001>.
- A. Maissonial, P. Serafin, M. Traukia, E. Debiton, V. Thery, D.J. Aitken, P. Lemoine, B. Viossat, A. Gautier, Click chelators for platinum-based anticancer drugs, *Eur. J. Inorg. Chem.* 2 (2008) 298–305, <https://doi.org/10.1002/ejic.200700849>.
- G. Aromi, L.A. Barrios, O. Roubeau, P. Gamez, Triazoles and tetrazoles: prime ligands to generate remarkable coordination materials, *Coord. Chem. Rev.* 255 (2011) 485–546, <https://doi.org/10.1016/j.ccr.2010.10.038>.
- A.C. García-Álvarez, E. Bernabé-Pablo, J. Barroso-Flores, V. Jancik, D. Martínez-Otero, T. Morales-Juárez, M. Moya-Cabrera, Multinuclear rare-earth metal complexes supported by chalcogen-based 1,2,3-triazole, *Polyhedron* 135 (2017) 10–16, <https://doi.org/10.1016/j.poly.2017.06.047>.
- D. Astrura, L. Liang, A. Rapakousiou, J. Ruiz, Click dendrimers and triazole related aspects: catalysts, mechanism, synthesis, and functions. A bridge between dendritic architectures and nanomaterials, *Acc. Chem. Res.* 45 (2012) 630–640, <https://doi.org/10.1021/ar200235m>.
- N.T.N. Anh, A.D. Chowdhury, R.A. Doong, Highly sensitive and selective detection of mercury ions using N, S-codoped graphene quantum dots and its paper strip based sensing application in wastewater, *Sensor. Actuator. B* 252 (2017) 1169–1178, <https://doi.org/10.1016/j.snb.2017.07.177>.
- S. Squadrone, A. Benedetto, P. Brizio, M. Prearo, M. Abete, Mercury and selenium in European catfish (*Silurus glanis*) from Northern Italian Rivers: can molar ratio be a predictive factor for mercury toxicity in a top predator? *Chemosphere* 119 (2015) 24–30, <https://doi.org/10.1016/j.chemosphere.2014.05.052>.
- J.Y. Chen, W. Su, E.J. Wang, Highly selective ratiometric fluorescent probe for  $\text{Hg}^{2+}$  based on fluorescence Resonance Energy Transfer between 1,8-naphthalimide and rhodamine B, *Chem. J. Chin. Univ.* 37 (2016) 232–238, <https://doi.org/10.7503/cjcu.20150563>.
- J. Ge, X. Geng, Y.H. Du, J.J. Chen, L. Zhang, D.M. Bai, D.Y. Ji, Y.L. Hu, Z.H. Li, Highly sensitive fluorescence detection of mercury (II) ions based on WS2nanosheets and T7 exonuclease assisted cyclic enzymatic amplification, *Sensor. Actuator. B* 249 (2017) 189–194, <https://doi.org/10.1016/j.snb.2017.04.094>.
- M. Ghanei-Motlagh, M.A. Taher, A. Heydari, R. Ghanei-Motlagh, V.K. Gupta, A novel voltammetric sensor for sensitive detection of mercury(II) ions using glassy carbon electrode modified with graphene-based ion imprinted polymer, *Mater. Sci. Eng.* 63 (2016) 367–375, <https://doi.org/10.1016/j.msec.2016.03.005>.
- H. Huang, Y.H. Weng, L.H. Zheng, B.X. Yao, W. Weng, X.C. Lin, Nitrogen-doped carbon quantum dots as fluorescent probe for “off-on” detection of mercury ions, L-cysteine and iodide ions, *J. Colloid Interface Sci.* 506 (2017) 373–378, <https://doi.org/10.1016/j.jcis.2017.07.076>.
- N. Amiri, M.K. Rofouei, J.B. Ghasemi, Multivariate optimization, preconcentration and determination of mercury ions with (1-(p-acetyl phenyl)-3-(o-methyl benzoate)) triazine in aqueous samples using ICP-AES, *Anal. Methods* 8 (2016) 1111–1119, <https://doi.org/10.1039/C5AY03169A>.
- H. Wang, B.B. Chen, S.Q. Zhu, Chip-based magnetic solid-phase microextraction online coupled with microHPLC-ICPMS for the determination of mercury species in cells, *Anal. Chem.* 88 (2016) 796–802, <https://doi.org/10.1021/acs.analchem.5b03130>.
- Q.M. Wang, W. Gao, X.H. Tang, Y. Liu, Y. Li, A fluorescence turn-on sensor for aluminum ion by a naphthaldehyde derivative, *J. Mol. Struct.* 1109 (2016) 127–130, <https://doi.org/10.1016/j.molstruc.2015.12.076>.
- Y.W. Wang, L.X. Wang, F.P. An, H. Xu, Z.J. Yin, S.R. Tang, H.H. Yang, H.B. Song, Graphitic carbon nitride supported platinum nanocomposites for rapid and sensitive colorimetric detection of mercury ions, *Anal. Chim. Acta* 980 (2017) 72–78, <https://doi.org/10.1016/j.aca.2017.05.019>.
- G. Liu, J. Shao, A C2-symmetric ratiometric fluorescence and colorimetric anion sensor based on pyrrole derivative, *J. Lumin.* 131 (2011) 1397–1400, <https://doi.org/10.1016/j.jlumin.2011.03.001>.
- L. Cao, C.M. Jia, Y. Huang, Q. Zhang, N. Wang, Y.L. Xue, D.L. Du, A highly selective fluorescence turn-on detection of  $\text{Al}^{3+}$  and  $\text{Ca}^{2+}$  based on a coumarin-modified rhodamine derivative, *Tetrahedron Lett.* 55 (2014) 4062–4066, <https://doi.org/10.1016/j.tetlet.2014.06.015>.
- A. Dhara, A. Jana, S.K. Mandal, A.R. Khuda-Bukhsh, N. Guchhait, S.K. Kar, A unique rhodamine-based ‘off-on’ molecular spy for selective detection of trivalent aluminum and chromium ions: synthesis, crystal structure and spectroscopic properties along with living cell imaging, *Inorg. Chim. Acta.* 423 (2014) 454–461, <https://doi.org/10.1016/j.ica.2014.09.008>.
- H. Yang, Z.G. Zhou, K.W. Huang, M.X. Yu, F.Y. Li, T. Yi, C.H. Huang, Multisignaling optical-electrochemical sensor for  $\text{Hg}^{2+}$  based on a rhodamine derivative with a ferrocene unit, *Org. Lett.* 9 (2007) 4729–4732, <https://doi.org/10.1021/oi7020143>.
- L. Wang, D.D. Ye, W.X. Li, Y.Y. Liu, L.H. Li, W.L. Zhang, L. Ni, Fluorescent and colorimetric detection of Fe(III) and Cu(II) by a difunctional rhodamine-based probe, *Spectrochim. Acta, Part A* 183 (2017) 291–297, <https://doi.org/10.1016/j.saa.2017.04.056>.
- Y. Chen, B. Chen, Y.F. Han, A novel rhodamine-based fluorescent probe for the fluorogenic and chromogenic detection of  $\text{Pd}^{2+}$  ions and its application in live-cell imaging, *Sensor. Actuator. B* 237 (2016) 1–7, <https://doi.org/10.1016/j.snb.2016.06.067>.
- H.M. Kang, C.B. Fan, H.T. Xu, G. Liu, S.Z. Pu, A highly selective fluorescence switch for  $\text{Cu}^{2+}$  and  $\text{Fe}^{3+}$  based on a new diarylethene with a triazole-linked rhodamine 6G

- unit, *Tetrahedron* 74 (2018) 4390–4399, <https://doi.org/10.1016/j.tet.2018.07.002>.
- [25] Z.Q. Yan, G. Wei, S.Y. Guang, M.M. Xu, X. Ren, R.L. Wu, G. Zhao, F.Y. Ke, H.Y. Xu, A multidentate ligand chromophore with rhodamine-triazole-pyridine units and its acting mechanism for dual-mode visual sensing trace  $\text{Sn}^{2+}$ , *Dyes Pigments* 159 (2018) 542–550, <https://doi.org/10.1016/j.dyepig.2018.07.028>.
- [26] S. Erdemir, O. Kocuyigit, S. Malkondu, Detection of  $\text{Hg}^{2+}$  ion in aqueous media by new fluorometric and colorimetric sensor based on triazole-rhodamine, *J. Photochem. Photobiol., A* 309 (2015) 15–21, <https://doi.org/10.1016/j.jphotochem.2015.04.017>.
- [27] K. Wechakorna, K. Suksenc, P. Piyachaturawat, P. Kongsaree, Rhodamine-based fluorescent and colorimetric sensor for zinc and its application in bioimaging, *Sensor. Actuator. B* 228 (2016) 270–277, <https://doi.org/10.1016/j.snb.2016.01.045>.
- [28] S. Erdemir, S. Malkondu, A simple triazole-based “turn on” fluorescent sensor for  $\text{Al}^{3+}$  ion in  $\text{MeCN-H}_2\text{O}$  and  $\text{F}^-$  ion in  $\text{MeCN}$ , *J. Lumin.* 158 (2015) 401–406, <https://doi.org/10.1016/j.jlumin.2014.10.043>.
- [29] Y.S. Jeong, J.Y. Yoon, Recent progress on fluorescent chemosensors for metal ions, *Inorg. Chim. Acta* 381 (2012) 2–14, <https://doi.org/10.1016/j.ica.2011.09.011>.
- [30] G.H. Ding, L.Y. Wu, H.J. Feng, Y.P. Liu, J.L. Li, H.Z. Si, X.J. Yao, M.X. He, W.Y. He, The specific binding of a new 1,2,3-triazole to three blood proteins and its appended rhodamine complex for selective detection of  $\text{Hg}^{2+}$ , *Spectrochim. Acta, Part A* 228 (2020) 117728 In press <https://doi.org/10.1016/j.saa.2019.117728>.
- [31] J.L. Li, G.H. Ding, Y.Y. Niu, L.Y. Wu, H.J. Feng, W.Y. He, The structural properties of 5-methyl-2-phenyl-2H-1,2,3-triazole-4-carboxylic acid and chromogenic mechanism on its rhodamine B derivatives to  $\text{Hg}^{2+}$  ions, *Spectrochim. Acta, Part A* 200 (2018) 127–135, <https://doi.org/10.1016/j.saa.2018.04.009>.
- [32] B. Khan, A. Hameed, A. Minhaz, M.R. Shah, Synthesis and characterisation of calix [4]arene based bis(triazole)-bis(hexahydroquinoline): probing highly selective fluorescence quenching towards mercury ( $\text{Hg}^{2+}$ ) analyte, *J. Hazard Mater.* 347 (2018) 349–358, <https://doi.org/10.1016/j.jhazmat.2018.01.022>.
- [33] Q.Y. Cao, Y.M. Han, H.M. Wang, Y. Xie, A new pyrenyl-appended triazole for fluorescent recognition of  $\text{Hg}^{2+}$  ion in aqueous solution, *Dyes Pigments* 99 (2013) 798–802, <https://doi.org/10.1016/j.dyepig.2013.07.005>.
- [34] M. Sulak, A.N. Kursunlu, B. Girgin, Ö. Karakuş, E. Güler, A highly selective fluorescent sensor for mercury (II) ion based on Bodipy and Calix[4]arene bearing triazolenaphthylene groups; synthesis and photophysical investigations, *J. Photochem. Photobiol., A* 349 (2017) 129–137, <https://doi.org/10.1016/j.jphotochem.2017.09.022>.
- [35] J. Hua, M. Zhang, L.B. Yu, Y. Ju, Synthesis and binding ability of 1,2,3-triazole-based triterpenoid receptors for recognition of  $\text{Hg}^{2+}$  ion, *Bioorg. Med. Chem. Lett.* 20 (2010) 4342–4345, <https://doi.org/10.1016/j.bmcl.2010.06.079>.
- [36] L.Y. Wang, G.P. Fang, D.C. Ye, D.R. Cao, Carbazole and triazole-containing conjugated polymer as a visual and fluorometric probe for iodide and mercury, *Sensor. Actuator. B Chem.* 195 (2014) 572–580, <https://doi.org/10.1016/j.snb.2014.01.081>.
- [37] K.H. Chen, C.Y. Lu, H.J. Cheng, S.J. Chen, C.H. Hu, A.T. Wu, A pyrenyl-appended triazole-based ribose as a fluorescent sensor for  $\text{Hg}^{2+}$  ion, *Carbohydr. Res.* 345 (2010) 2557–2561, <https://doi.org/10.1016/j.carres.2010.09.010>.
- [38] A. Kumar, P.S. Pandey, Steroidal 1,2,3-triazole-based sensors for  $\text{Hg}^{2+}$  ion and their logic gate behaviour, *Tetrahedron Lett.* 50 (2009) 5842–5845, <https://doi.org/10.1016/j.tetlet.2009.08.007>.
- [39] S. Erdemir, O. Kocuyigit, S. Malkondu, Detection of  $\text{Hg}^{2+}$  ion in aqueous media by new fluorometric and colorimetric sensor based on triazole-rhodamine, *J. Photochem. Photobiol., A* 309 (2015) 15–21, <https://doi.org/10.1016/j.jphotochem.2015.04.017>.
- [40] B.X. Shen, Y. Qian, Click synthesis,  $\text{Hg}^{2+}$  sensor and intramolecular fluorescence resonance energy transfer in novel BODIPY dendrons, *Sensor. Actuator. B Chem.* 239 (2017) 226–234, <https://doi.org/10.1016/j.snb.2016.08.004>.
- [41] Y.L. Lv, L.L. Zhu, H. Liu, Y.S. Wu, Z.L. Chen, H.B. Fu, Z.Y. Tian, Single-fluorophore-based fluorescent probes enable dual-channel detection of  $\text{Ag}^+$  and  $\text{Hg}^{2+}$  with high selectivity and sensitivity, *Anal. Chim. Acta* 839 (2014) 74–82, <https://doi.org/10.1016/j.aca.2014.06.010>.
- [42] D. Mandal, A. Thakur, S. Ghosh, A triazole tethered ferrocene derivative as a selective chemosensor for mercury(II) in aqueous environment, *Polyhedron* 52 (2013) 1109–1117, <https://doi.org/10.1016/j.poly.2012.06.060>.
- [43] A. Thakur, D. Mandal, S. Ghosh, A triazole based triferrocene derivative as a multiresponsive chemosensor for  $\text{Hg}(\text{II})$  ion and a redox chemosensor for  $\text{H}_2\text{PO}_4^-$  ion, *J. Organomet. Chem.* 726 (2013) 71–78, <https://doi.org/10.1016/j.jorganchem.2012.11.031>.
- [44] N.J. Wang, C.M. Sun, W.S. Chung, A specific and ratiometric chemosensor for  $\text{Hg}^{2+}$  based on triazole coupled ortho-methoxyphenylazocalix [4]arene, *Tetrahedron* 67 (2011) 8131–8139, <https://doi.org/10.1016/j.tet.2011.08.052>.
- [45] Y.B. Ruan, S. Maisonneuve, J. Xie, Highly selective fluorescent and colorimetric sensor for  $\text{Hg}^{2+}$  based on triazole-linked NBD, *Dyes Pigments* 90 (2011) 239–244, <https://doi.org/10.1016/j.dyepig.2011.01.004>.
- [46] S.R. Bhatta, V. Bheemireddy, G. Vijaykumar, A. Thakur, Triazole appended mono and 1,1'-di-substituted ferrocene-naphthalene conjugates: highly selective and sensitive multi-responsive probes for  $\text{Hg}(\text{II})$ , *Sensor. Actuator. B Chem.* 240 (2017) 640–650, <https://doi.org/10.1016/j.snb.2016.09.022>.
- [47] L.Y. Wu, S. Guo, X.H. Wang, Z.F. Guo, G.G. Yao, Q. Lin, M.S. Wu, Tandem synthesis of 2-aryl-1,2,3-triazoles from  $\alpha$ -arylhydrazonoketones with  $\text{NH}_4\text{OAc}$  via copper-catalyzed aerobic oxidation, *Tetrahedron Lett.* 56 (2015) 2145–2148, <https://doi.org/10.1016/j.tetlet.2015.03.019>.
- [48] F. Ge, H. Ye, J.Z. Luo, S. Wang, Y.J. Sun, B.X. Zhao, J.Y. Miao, A new fluorescent and colorimetric chemosensor for  $\text{Cu}(\text{II})$  based on rhodamine hydrazone and ferrocene unit, *Sensor. Actuator. B* 181 (2013) 215–220, <https://doi.org/10.1016/j.snb.2013.01.048>.
- [49] A. Frisch, R. Dennington, T. Keith, J. Millam, A. Nielsen, A. Holder, J. Hiscoks, *Gauss View Version 5 User Manual*, Gaussian Inc., Wallingford, CT, USA, 2009.
- [50] M.A.M. El-Mansy, Quantum chemical studies on structural, vibrational, nonlinear optical properties and chemical reactivity of indigo carmine dye, *Spectrochim. Acta, Part A* 183 (2017) 284–290, <https://doi.org/10.1016/j.saa.2017.04.047>.
- [51] X.X. Wang, X.L. Li, W. Shi, S. Wei, J.P. Giesy, H.X. Yu, Y.L. Wang, Docking and CoMSIA studies on steroids and non-steroidal chemicals as androgen receptor ligands, *Ecotoxicol. Environ. Saf.* 89 (2013) 143–149, <https://doi.org/10.1016/j.ecoenv.2012.11.020>.
- [52] Y.C. Chou, The low-lying singlet electronic excited states of  $\text{ZrO}_2$ : a symmetry adapted cluster-configuration interaction (SAC-Cl) study, *Comput. Theor. Chem.* 1069 (2015) 112–118, <https://doi.org/10.1016/j.comptc.2015.07.021>.
- [53] S. Shahab, M. Sheikhi, L. Filippovich, R.K.E. Dikumar, H. Yahyaee, M. Khaleghian, Synthesis, geometry optimization, spectroscopic investigations (UV/Vis, excited states, FT-IR) and application of new azomethine dyes, *J. Mol. Struct.* 1148 (2017) 134–149, <https://doi.org/10.1016/j.molstruc.2017.07.036>.
- [54] X.H. Li, H.L. Cui, R.Z. Zhang, X.Z. Zhang, Theoretical investigation on the non-linear optical properties, vibrational spectroscopy and frontier molecular orbital of (E)-2-cyano-3-(3-hydroxyphenyl)acrylamide molecule, *Spectrochim. Acta Part A* 137 (2015) 321–327, <https://doi.org/10.1016/j.saa.2014.08.036>.
- [55] O. Mihçokur, T. Ozpozan, Molecular structure, vibrational spectroscopic analysis (IR & Raman), HOMO-LUMO and NBO analysis of anti-cancer drug sunitinib using DFT method, *J. Mol. Struct.* 1149 (2017) 27–41, <https://doi.org/10.1016/j.molstruc.2017.07.064>.
- [56] N. Anusuya, P. Sounthari, J. Saranya, K. Paramswar, S. Chitra, Quantum chemical study on the corrosion inhibition property of some heterocyclic azole derivatives, *Orient. J. Chem.* 31 (2015) 1741–1750, <https://doi.org/10.13005/ojc/310355>.
- [57] T.K. Kuruvilla, J.C. Prasana, S. Muthu, J. George, S.A. Mathew, Quantum mechanical and spectroscopic (FT-IR, FT-Raman) study, NBO analysis, HOMO-LUMO, first order hyperpolarizability and molecular docking study of methyl[(3R)-3-(2-methylphenoxy)-3-phenylpropyl]amine by density functional method, *Spectrochim. Acta Part A* 188 (2018) 382–393, <https://doi.org/10.1016/j.saa.2017.07.029>.
- [58] A. Rauk, *Orbital Interaction Theory of Organic Chemistry*, second ed., Wiley Interscience, New York, 2001.
- [59] A. Streitwieser Jr., *Molecular Orbital Theory for Organic Chemistry*, Wiley, New York, 1961.
- [60] A.R. Chaudhry, R. Ahmed, A. Irfan, S. Muhammad, A. Shaari, A.G. Al-Sehemi, Effect of heteroatoms substitution on electronic, photophysical and charge transfer properties of naphtha [2,1-b:6,5-b'] difuran analogues by density functional theory, *Comput. Theor. Chem.* 1045 (2014) 123–134, <https://doi.org/10.1016/j.comptc.2014.06.028>.
- [61] H.A. Kurtz, J.P. Stewart, K.M. Dieter, Calculation of the nonlinear optical properties of molecules, *J. Comput. Chem.* 11 (1990) 82–87, <https://doi.org/10.1002/jcc.540110110>.
- [62] J.G. Xu, Z.B. Wang, *Fluorescence Analysis*, third ed., Science Press, Beijing, 2006.
- [63] M.H. Zhu, P. Hu, *Instrumental Analysis*, fourth ed., Higher Education Press, Beijing, 2008.
- [64] W.M. Yan, Q.Y. Wang, Q. Lin, M.Y. Li, J.L. Petersen, X.D. Shi, N-2-Aryl-1,2,3-triazoles: a novel class of UV/Blue-light-emitting fluorophores with tunable optical properties, *Chem. Eur. J.* 17 (2011) 5011–5018, <https://doi.org/10.1002/chem.201002937>.
- [65] V. Tekuri, D.R. Trivedi, A new colorimetric chemosensors for  $\text{Cu}^{2+}$  and  $\text{Cd}^{2+}$  ions detection: application in environmental water samples and analytical method validation, *Anal. Chim. Acta* 972 (2017) 81–93, <https://doi.org/10.1016/j.aca.2017.03.035>.
- [66] J. Zhang, C.W. Yu, S.Y. Qian, G. Lu, J.L. Chen, A selective fluorescent chemosensor with 1, 2, 4-triazole as subunit for  $\text{Cu}(\text{II})$  and its application in imaging  $\text{Cu}(\text{II})$  in living cells, *Dyes Pigments* 92 (2012) 1370–1375, <https://doi.org/10.1016/j.dyepig.2011.09.020>.
- [67] K. Shaha, N.U. Aina, F. Ahmeda, I. Anis, M.R. Shah, A new highly selective chemosensor for the detection of iron ion in aqueous medium based on click generated triazole, *Sensor. Actuator. B* 249 (2017) 515–522, <https://doi.org/10.1016/j.snb.2017.04.120>.
- [68] C. Wu, Y. Ikejiri, J.L. Zhao, X.K. Jiang, X.L. Ni, X. Zeng, C. Redshaw, T. Yamato, A pyrene-functionalized triazole-linked hexahomotrioxacalix[3]arene as a fluorescent chemosensor for  $\text{Zn}^{2+}$  ions, *Sensor. Actuator. B* 228 (2016) 480–485, <https://doi.org/10.1016/j.snb.2016.01.051>.
- [69] X. Chen, T. Pradhan, F. Wang, J.S. Kim, J. Yoon, Fluorescent chemosensors based on spiro-opening of xanthenes and related derivatives, *Chem. Rev.* 112 (2012) 1910–1956, <https://doi.org/10.1021/cr200201v>.
- [70] R.Y. Wang, X.H. Zhou, H.C. Shi, Y. Luo, T-T mismatch-driven biosensor using triple functional DNA-protein conjugates for facile detection of  $\text{Hg}^{2+}$ , *Biosens. Bioelectron.* 78 (2016) 418–422, <https://doi.org/10.1016/j.bios.2015.11.082>.
- [71] A.G. Memon, Y.P. Xing, X.H. Zhou, R.Y. Wang, L.H. Liu, S.Y. Zeng, M. He, M. Ma, Ultrasensitive colorimetric aptasensor for  $\text{Hg}^{2+}$  detection using Exo-III assisted target recycling amplification and unmodified AuNPs as indicators, *J. Hazard Mater.* 384 (2020) 120948, <https://doi.org/10.1016/j.jhazmat.2019.120948>.
- [72] E.J. Olson, P. Buhlmann, Getting more out of a job plot: determination of reactant to product stoichiometry in cases of displacement reactions and n:n complex formation, *J. Org. Chem.* 76 (2011) 8406–8412, <https://doi.org/10.1021/jo201624p>.
- [73] Y.M. Yang, Q. Zhao, W. Feng, F.Y. Li, Luminescent chemodosimeters for bioimaging, *Chem. Rev.* 113 (2013) 192–270, <https://doi.org/10.1021/cr2004103>.
- [74] D.T. Quang, J.S. Kim, Fluoro- and chromogenic chemodosimeters for heavy metal

- ion detection in solution and biospecimens, *Chem. Rev.* 110 (2010) 6280–6301, <https://doi.org/10.1021/cr100154p>.
- [75] D.G. Cho, J.L. Sessler, Modern reaction-based indicator systems, *Chem. Soc. Rev.* 38 (2009) 1647–1662, <https://doi.org/10.1039/B804436H>.
- [76] C.C. Jiang, M. Wang, Y.X. Wang, X.N. Tang, Y.M. Zhang, H. Zhang, L. Ma, J.Y. Wang, Synthesis and evaluation of two novel rhodamine-based fluorescence probes for specific recognition of  $\text{Fe}^{3+}$  ion, *Tetrahedron Lett.* 58 (2017) 2560–2565, <https://doi.org/10.1016/j.tetlet.2017.05.052>.
- [77] L. Lan, Q. Niu, Z. Guo, H. Liu, T. Li, Highly sensitive and fast responsive turn-on fluorescent sensor for selectively sensing  $\text{Fe}^{3+}$  and  $\text{Hg}^{2+}$  in aqueous media based on an oligothiophene derivative and its application in real water samples, *Sensor. Actuator. B* 244 (2017) 500–508, <https://doi.org/10.1016/j.snb.2017.01.042>.
- [78] S. Erdemir, S. Malkondu, O. Alici, A highly selective and sensitive benzothiazole-based ‘turn-on’ fluorescent sensor for  $\text{Hg}^{2+}$  ion, *Color. Technol.* 131 (2015) 32–37, <https://doi.org/10.1111/cote.12122>.